Signal Processing 129 (2016) 67–81

Contents lists available at ScienceDirect

Signal Processing

journal homepage: www.elsevier.com/locate/sigpro

Frequency estimation of sinusoids from nonuniform samples

Syed Alam Abbas[a,*], Qiyu Sun[b], Hassan Foroosh[a]

[a] Department of Electrical Engineering and Computer Science, University of Central Florida, Orlando, FL 32816, United States
[b] Department of Mathematics, University of Central Florida, Orlando, FL 32816, United States

ARTICLE INFO

Article history:
Received 24 October 2015
Received in revised form
17 May 2016
Accepted 23 May 2016
Available online 27 May 2016

Keywords:
Frequency estimation
Mixture of sinusoids
Nonuniform samples
Adaptive notch filter
Cramer–Rao bound
Dynamic systems
Local convergence
Tracking frequency

ABSTRACT

Sinusoid signals with multiple frequencies appear in various systems and their frequencies may carry some important features. Frequency estimation from their discrete samples is one of the fundamental problems and many frequency estimators have been proposed for uniform sampling setting. In this paper, frequency estimators based on adaptive notch filtering are proposed for nonuniform sampling setting. We observe that some dynamic systems associated with adaptive notch filters can be solved in nonuniformly sampled time steps with high accuracy. This leads us to propose a digital adaptive notch filtering method to estimate frequency of a sinusoidal signal with single frequency from its nonuniform samples. The proposed method exhibits convergent and robust frequency estimation in the presence of random sampling noises, and its variance is comparable to the Cramer–Rao lower bound in the presence of additive white noise. The above method designed for single frequency estimation could track abrupt single frequency change of an input signal, but it is not applicable directly for multiple frequency estimation. Our simulations show that the proposed estimators have robust performance for sinusoidal signals with multiple distinct frequencies, and they can be used to separate two very close frequencies of an input signal in a highly noisy sampling environment.

© 2016 Elsevier B.V. All rights reserved.

1. Introduction

Consider a mixture of sinusoidal signals, whose kth component has amplitude A_k, frequency θ_k and phase ϕ_k, $1 \le k \le K$,

$$y(t) = \sum_{k=1}^{K} A_k \sin(\theta_k t + \phi_k). \tag{1.1}$$

Such sinusoidal signals are encountered in active noise and vibration control, wireless communications, audio, radar and sonar signal processing [1–4]. In telecommunication systems, the frequencies θ_k, $1 \le k \le K$, contain carrier's phase information necessary for synchronization of demodulators or other components of a receiver system.

The estimation problem of frequencies θ_k, $1 \le k \le K$, of the signal y is a fundamental problem in systems theory with many applications. It has been intensively studied in signal processing, instrumentation and measurements, and control theory. Many frequency estimators have been proposed, including adaptive notch filtering, time frequency representation, phase locked loop, eigensubspace tracking, extended Kalman filtering, internal model method, etc., see [5–8] and references therein.

Most of existing estimators are derived for uniformly sampled data $y(n\Delta T)$, $n \ge 0$, with uniform sampling frequency $1/\Delta T$, and often only for a single frequency, i.e., $K=1$. In this paper, we consider multiple frequency estimation problem of the signal y from its nonuniform samples,

$$z_n = y(T_n) + w_n, \quad n \ge 0, \tag{1.2}$$

corrupted by additive noises w_n, where T_n, $n \ge 0$, are sampling times.

Nonuniform sampling arises in many applications, such as computer graphics, frequency scanning interferometry, magnetic resonance imaging, computer tomography scans and Radon imaging [9–14]. Uniform sampling is well studied and it has been widely used in engineering applications. However in some applications, nonuniform sampling is necessary and it has better performance. For instance, in antialiasing in computer graphics [15], better results can be obtained with random sampling instead of uniform sampling. The sampling operation could be costly, and a low number of samples (but not necessarily uniform) is more desirable. For instance, in frequency scanning interferometry, the sampling effort is measured by the acquisition time at a given point, and the optimal sampling scheme is usually nonuniform [16]. Nonuniformly sampled data are harder to analyze and the related methods, even for a "simple" task of obtaining the discrete nonuniform Fourier transform, are much more difficult and often

* Corresponding author.
E-mail addresses: syedalamabbas@knights.ucf.edu, syedalamabbas@gmail.com (A.A. Syed), qiyu.sun@ucf.edu (Q. Sun), foroosh@eecs.ucf.edu (H. Foroosh).

http://dx.doi.org/10.1016/j.sigpro.2016.05.024
0165-1684/© 2016 Elsevier B.V. All rights reserved.

iterative [9,17]. Several statistical frequency estimators (based on maximum likelihood estimation and filter banks) from nonuniformly sampled data have been proposed in the literature [11,18–23]. For nonuniform sampling problems in signal processing, the reader may refer to [24–26].

In many applications of signal processing, it is desirable to eliminate or extract sine waves from observed data or to estimate their unknown frequencies. Since the frequencies often vary with time, it is useful to apply adaptive notch filters (ANFs) that adapt their notch frequencies as a function of the observed time series, see [27,28] and references therein. The ANF method is one of the most suitable techniques to separate sinusoidal components of unknown frequencies buried in noise, and/or retrieve such periodic components [29–35]. It is robust in the presence of sampling noise and it is capable of changing the notch frequency accordingly. Various architectures have been proposed for the construction of adaptive notch filters, see for instance [1,36–41].

Frequency estimation problem using ANF is modeled as a nonlinear system identification of a dynamic system either in continuous time (CT) (e.g. [1]) or in discrete time (DT) (e.g. [29]). The CT model systems are native to the physical world, they have a built-in capability to cope with the nonuniformly sampled signal, and they offer certain advantages over purely DT model systems [45,46]. Compared to the DT model, direct estimation of CT models is usually stable, accurate and free from undesirable sensitivity problems, particularly at high sampling rates. The frequency estimator developed in this paper is based on ANFs, which are governed by some CT dynamic systems [29–35,42–44]. We mainly focus on a particular ANF governed by the following dynamic system:

$$\begin{cases} Dx_1 = x_2 \\ Dx_2 = -2\xi\theta x_2 - \theta^2 x_1 + \theta^2 y \\ D\theta = -\gamma(\theta^2 y - 2\xi\theta x_2)x_1, \end{cases} \tag{1.3}$$

where D represents the derivative with respect to time t, x_1, x_2, θ are states of the system, y is the excitation sinusoidal input with single frequency θ_0 (i.e., $K=1$ in (1.1)), ξ is the notch depth, and γ is the adaptation speed. The above system of nonlinear ordinary differential equations (ODE) has good noise rejection capability. It was proposed by Regalia in [1] as a DT filter, it was later adapted by Bodson and Douglas [42] for a CT system, and finally a modified version was proposed by Hsu et al. [29]. We have chosen this dynamic system due to its superior performance compared to the other systems that can be used with a similar discretization procedure, see Section 2.5 for performance comparison.

The main difficulty in handling CT dynamic systems directly is the problem of evaluating derivatives of the input signal (with unknown parameters) from its nonuniform samples numerically, the numerical differentiation process in a highly noisy environment is usually unstable and impractical [47–49]. In this paper, we propose a Taylor-like approximation of the dynamic system (1.3) that is robust to noise and achieves high accuracy. Based on the above approximation, we introduce an ANF method (2.13) to estimate the frequency of a sinusoidal signal from its nonuniform samples. The proposed discrete ANF method reconciles the merits of CT models while restricting itself to operate directly on the DT data.

This paper is organized as follows. Section 2 discusses a Taylor-like approximation technique to solve the system (1.3) and a frequency estimation of the unknown input signal with single frequency. We propose the frequency estimator (2.13), perform the local stability analysis, and study its convergence, noise characteristics, statistical properties, and comparison to the conventional ODE solver for the dynamic systems associated with the ANF methods. We also perform a comparison of our method with a state of the art discrete ANF [40]. Section 3 describes extensions of the single frequency estimator (2.13) to multiple frequency estimations with two configurations, the cascade ANF method and the prefiltering ANF method. The two proposed multiple frequency estimators have robust performance for sinusoidal signals with multiple distinct frequencies or related harmonic frequencies. Most of the known frequency estimators have poor performance when input signal has two very close frequencies in a highly noisy environment, a pathological case where the estimation error is related to both the difference in the frequency and the noise level, see [50] and references therein. Our simulation indicates that the cascade ANF method has sound performance even in the separation of very close frequencies of the input signal in a highly noisy sampling environment. We close the paper with concluding remarks in Section 4.

Notation: We use Euler notation for expressing derivatives, D^n instead of D_t^n to denote the nth derivative with respect to time t.

2. Single frequency estimation

Consider a sinusoidal input,

$$y(t) = A\sin(\theta_0 t + \phi), \tag{2.1}$$

where A, θ_0, ϕ are its amplitude, frequency, and phase respectively. In the first subsection, we propose a discrete ANF method to estimate frequency θ_0 of the sinusoid signal y from its nonuniform samples,

$$z_n = y(T_n) + w_n, \quad n \geq 0, \tag{2.2}$$

corrupted by additive noise w_n at sampling times T_n, $n \geq 0$. Then in the next four subsections, we discuss local stability, convergence, approximation error, statistical characterization, and extensions of the proposed ANF method. We also compare the performance of our approach (2.13) with some of the existing ANF methods for estimating frequency in Section 2.2 and 2.5.

2.1. The proposed method

The dynamical system (1.3) converges to its unique periodic orbit,

$$\left[x_1,\ x_2,\ \theta\right]^T = \left[\frac{-A\cos(\theta_0 t+\phi)}{2\xi},\ \frac{A\theta_0\sin(\theta_0 t+\phi)}{2\xi},\ \theta_0\right]^T, \tag{2.3}$$

when the adaption speed γ satisfies

$$0 < \gamma < 4\xi/A^2 \tag{2.4}$$

[29] . The dynamical system (1.3) can be rewritten as follows:

$$D\mathbf{X} = \mathbf{F}(t, \mathbf{X}), \tag{2.5}$$

where $\mathbf{X} = [x_1, x_2, \theta]^T$ is the state of the system, and

$$\mathbf{F}(t, \mathbf{X}) = \left[x_2,\ -2\xi\theta x_2 - \theta^2 x_1 + \theta^2 y,\ \gamma(2\xi\theta x_2 - \theta^2 y)x_1\right]^T$$

is a real analytic function of t and $\mathbf{X}$. Therefore $\mathbf{X}(t)$ is real analytic by the Cauchy–Kovalevskaya theorem [51, Theorem 2 of Chapter 4], and it has the following Taylor expansion:

$$\mathbf{X}(t) = \sum_{k=0}^{m} \frac{D^k\mathbf{X}(T_n)}{k!}t^k + \int_{T_n}^{t} D^m\mathbf{F}(s, \mathbf{X}(s))\frac{(t-s)^m}{m!}ds \tag{2.6}$$

for all $T_n \leq t \leq T_{n+1}$ and $m \geq 0$.

For an input signal of sinusoidal type, we observe that the state vector $\mathbf{X}(t)$ of the dynamical system (1.3) can be approximated by Taylor polynomials $\sum_{k=0}^{m} D^k\mathbf{X}(T_n)(t-T_n)^k/k!$ of low order $m \leq 4$,

$$\mathbf{X}(t) \approx \sum_{k=0}^{m} \frac{D^k \mathbf{X}(T_n)}{k!}(t - T_n)^k =: \mathbf{X}_{m,n}(t), \quad T_n \le t \le T_{n+1}, \tag{2.7}$$

when the maximal sampling gap $\max_n(T_{n+1} - T_n)$ is small, which in turn depends on the signal frequencies. The problem how to choose the maximal sampling gap and the choice of model order m is discussed further in Section 2.3, cf. (2.23), where it is shown to be dependent on the signal frequency θ.

For expressing Taylor polynomial approximation $\mathbf{X}_{m,n}(t)$, $m \le 4$, explicitly, we introduce few auxiliary variables $x_3 = \theta^2$, $x_4 = x_3 y$, $x_5 = 2\xi\theta x_2$ and $x_6 = x_1 x_3$. Consider the derivatives of order up to 4:

1st order derivatives,

$$\begin{cases} Dx_1 = x_2 \\ Dx_2 = x_4 - x_5 - x_6 \\ D\theta = -\gamma(x_4 - x_5)x_1 \\ Dx_3 = 2\theta D\theta \\ Dx_4 = x_3 Dy + y Dx_3 \\ Dx_5 = 2\xi(\theta Dx_2 + x_2 D\theta) \\ Dx_6 = x_1 Dx_3 + x_3 Dx_1. \end{cases} \tag{2.8}$$

2nd order derivatives,

$$\begin{cases} D^2x_1 = Dx_2 \\ D^2x_2 = Dx_4 - Dx_5 - Dx_6 \\ D^2\theta = -\gamma\{(x_4 - x_5)Dx_1 + x_1(Dx_4 - Dx_5)\} \\ D^2x_3 = 2\left\{\theta D^2\theta + (D\theta)^2\right\} \\ D^2x_4 = -x_3^2 y + 2Dy Dx_3 + y D^2x_3 \\ D^2x_5 = 2\xi(\theta D^2x_2 + 2Dx_2 D\theta + x_2 D^2\theta) \\ D^2x_6 = x_1 D^2x_3 + 2Dx_1 Dx_3 + x_3 D^2x_1. \end{cases} \tag{2.9}$$

3rd order derivatives,

$$\begin{cases} D^3x_1 = D^2x_2 \\ D^3x_2 = D^2x_4 - D^2x_5 - D^2x_6 \\ D^3\theta = -\gamma\{(x_4 - x_5)D^2x_1 + 2(Dx_4 - Dx_5)Dx_1 \\ \qquad + x_1(D^2x_4 - D^2x_5)\} \\ D^3x_3 = 2\{\theta D^3\theta + 3D\theta D^2\theta\} \\ D^3x_4 = -x_3(\theta^2 Dy + 2\theta D\theta y) - 3x_4 Dx_3 + 3Dy D^2x_3 \\ \qquad + y D^3x_3 \\ D^3x_5 = 2\xi(\theta D^3x_2 + 3D^2x_2 D\theta + 3Dx_2 D^2\theta + x_2 D^3\theta) \\ D^3x_6 = x_1 D^3x_3 + 3D^2x_1 Dx_3 + 3Dx_1 D^2x_3 + x_3 D^3x_1. \end{cases} \tag{2.10}$$

4th order derivatives,

$$\begin{cases} D^4x_1 = D^3x_2 \\ D^4x_2 = D^3x_4 - D^3x_5 - D^3x_6 \\ D^4\theta = -\gamma\{(x_4 - x_5)D^3x_1 + 3(Dx_4 - Dx_5)D^2x_1 \\ \qquad + 3(D^2x_4 - D^2x_5)Dx_1 + x_1(D^3x_4 - D^3x_5)\}. \end{cases} \tag{2.11}$$

In the above computation of derivatives of high orders, we require knowledge of derivatives of the excitation sinusoidal signal y with unknown frequency θ_0. As the dynamical system (1.3) converges to its unique periodic orbit (2.3), we may replace the true frequency θ_0 by the third state θ, and the digital differentiator Dy of the sinusoidal signal y, with the product $-2\xi\theta x_1$. This leads to the following approximation of Dy, D^2y, D^3y, and D^4y:

$$\begin{cases} Dy = A\theta_0 \cos(\theta_0 t + \phi) \approx -2\xi\theta x_1 \\ D^2y = -\theta_0^2 y \approx -\theta^2 y \\ D^3y = -\theta_0^2 Dy \approx -\theta^2 Dy \\ D^4y = \theta_0^4 y \approx \theta^4 y. \end{cases} \tag{2.12}$$

Inspired by (2.3), (2.7) and (2.12), we propose the following discretized adaptive notch filtering of order m to solve our frequency estimation problem:

$$\mathbf{X}(T_{n+1}) = \sum_{k=0}^{m} \frac{D^k \mathbf{X}(T_n)}{k!}(\Delta T_n)^k, \quad n \ge 0, \tag{2.13}$$

where $2 \le m \le 4$, the derivatives of $\mathbf{X} = [x_1, x_2, \theta]^T$ are given in (2.8)–(2.11), and the ones for y are provided by (2.12). The problem of how to select the approximation order $2 \le m \le 4$ of the proposed discretization procedure will be discussed in Section 2.3.

2.2. Local stability analysis and convergence

In this section, we discuss the local stability of the proposed dynamic system, demonstrate convergence of the proposed method (2.13) in general sampling setting, and compare its performance to frequency estimation using the conventional Runge–Kutta method under uniform sampling setting [54].

To study the local stability of the discrete system (2.13), we introduce the following continuous autonomous 4th order system:

$$\begin{cases} Dx_1 = x_2 \\ Dx_2 = -2\xi\theta x_2 - \theta^2 x_1 + \theta^2 y \\ D\theta = -\gamma(\theta^2 y - 2\xi\theta x_2)x_1 \\ Dy = -2\xi\theta x_1, \end{cases} \tag{2.14}$$

where $X = [x_1, x_2, \theta, y]$ is the state vector of the system. The proposed system (2.14) is highly nonlinear and there is no explicit solution. Now we consider the behavior of the above system at one of the equilibrium points, provided that the system converges in the periodic orbit defined in (2.3). The linearized system near the equilibrium point X^* is given by

$$DX = JX, \tag{2.15}$$

where $z_1 = \theta y - x_2\xi$, $z_2 = \theta y - 2x_2\xi$, and

$$J = \begin{bmatrix} 0 & 1 & 0 & 0 \\ -\theta^2 & -2\theta\xi & 2z_2 - 2\theta_2 x_1 & \theta^2 \\ -\gamma\theta z_2 & 2\gamma\theta x_1\xi & -2\gamma x_1 z_1 & -\gamma\theta^2 x_1 \\ -2\theta\xi & 0 & -2x_1\xi & 0 \end{bmatrix}\Bigg|_{X^*}. \tag{2.16}$$

By Poincare–Lyapunov Theorem [53], the linearized system (2.15) at the equilibrium point X^* is stable if and only if all eigenvalues of J have nonpositive real part. For the pure excitation input sinusoidal signal $y = A\sin(\theta_0 t)$ (i.e., $\phi = 0$ in (2.1)), the equilibrium points of the continuous system (2.14) are

$$X_0 = \left[\frac{-A\cos(\theta_0 t)}{2\xi}, \frac{A\theta_0 \sin(\theta_0 t)}{2\xi}, \theta_0, A\sin(\theta_0 t)\right]. \tag{2.17}$$

Direct computation shows that the eigenvalues of the linearized matrix J at X_0 with $A=1$ and $t=1$ are

$$\lambda_1 = -\theta_0 i, \quad \lambda_2 = \theta_0 i, \quad \lambda_3 = \frac{\theta_0(\sqrt{\Delta} + 2\gamma\sin(2\theta_0) - 16\xi^2)}{16\xi},$$

and

$$\lambda_4 = \frac{\theta_0(-\sqrt{\Delta} + 2\gamma\sin(2\theta_0) - 16\xi^2)}{16\xi},$$

where $\Delta = 2(\gamma^2 - \gamma^2\cos(4\theta_0) + 128\xi^4 - 64\gamma\xi\cos^2(\theta_0) - 32\gamma\xi^2\sin(2\theta_0))$. The first two eigenvalues λ_1, λ_2 are purely imaginary. Therefore, for the local stability of the continuous system (2.14) at the equilibrium point X_0 in (2.17), we require that the third and fourth eigenvalues (depending on γ, ξ and θ at the equilibrium point X^*) have negative real parts.

Observe that λ_3 and λ_4 form the conjugate roots of a quadratic equation, where Δ is the discriminant. Thus, we can determine how to adjust the parameters γ and ξ for the local stability.

- For the case when $\Delta < 0$, the two eigenvalues λ_3, λ_4 occur as a complex conjugate pair and the stability will only depend on their real parts. This implies that the system (2.14) has local stability near the equilibrium point if,

$$\gamma < \frac{4\xi^2}{\sin\theta_0\cos\theta_0} \tag{2.18}$$

- When $\Delta = 0$ the two eigenvalues are real and $\lambda_3 = \lambda_4$, the stability will still depend on the same condition (2.18).
- For the case when $\Delta > 0$, eigenvalues λ_3, λ_4 are real and distinct. For the local stability of the system (2.14), we require that $\lambda_3 + \lambda_4 < 0$ and $\lambda_3\lambda_4 > 0$, which are equivalent to the following:

$$\gamma < \frac{4\xi^2}{\sin\theta_0\cos\theta_0} \quad \text{and} \quad \frac{\gamma\theta_0^2\cos^2\theta_0}{2\xi} > 0.$$

The last condition is satisfied simply by choosing $\gamma, \xi > 0$, and these parameters are by definition positive. Hence in all cases the local stability depends only on satisfying the stability condition (2.18), cf. the similar stability condition (2.4) in [29].

To study the local stability of the system (2.14) using experiments, we choose the adaption alertness parameters γ and noise sensitivity parameter ξ as in (2.4). For $\xi = 0.1$ and $\gamma = 0.001$, numerical simulation indicates that the third and fourth eigenvalues λ_3 and λ_4 remain strictly negative and negatively increasing about the $\theta_0 = 2\pi f_0$, where $f_0 \in [30, 300]$ Hz, see Fig. 1. For different values of parameters ξ and γ, one may find the range of frequencies so that the third and fourth eigenvalues have strictly negative real part, and hence the nonlinear dynamic system (2.14) is locally asymptotically stable. Thus with the use of both qualitative and quantitative techniques we have established the local stability of the proposed dynamic system. There are still mathematical difficulties to study stability for the proposed dynamic system (2.14) in the discrete setting using only the nonuniform sampling data (2.13). Our numerical results show that all trajectories starting close to the periodic orbit region will stay near the region when the approximation order is chosen appropriately and nonuniform sampling is taken with small sampling gap (depending on the signal frequency).

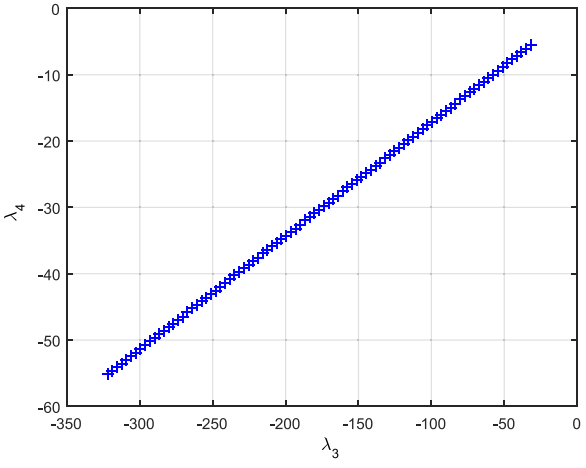

Fig. 1. Eigenvalue plot of the Jacobian system, $\xi = 0.1$, $\gamma = 0.001$ in a frequency range, $\theta_0 = 2\pi f_0$ where $f_0 \in [30, 300]$ Hz in steps of 3 Hz. The eigenvalues λ_3, λ_4 remain strictly <0 making the actual nonlinear system linearized locally at a point in the periodic orbit to be locally asymtotically stable.

The ANF technique governed by the dynamic system (1.3) is a globally convergent estimator with very high noise immunity [29]. The discretized version (2.13) is based on the observation that the evaluation of derivatives of the input excitation sinusoidal signal could be circumvented by using the interrelationship among the states of the dynamic system, see (2.12). The system (2.13) converges according to our analysis and simulations.

The discrete system (2.13) could be implemented for both nonuniformly or uniformly sampled data without any significant changes to its implementation. The simplest models for nonuniform sampling schemes are the jittered nonuniform sampling [22],

$$T_n = n\Delta T + \tau_n, \tag{2.19}$$

and the additive nonuniform sampling,

$$T_{n+1} = T_n + \tau_n, \tag{2.20}$$

where ΔT is the uniform sampling rate and τ_n is a family of identically distributed independent random variables with mean ΔT and small $\max_n \tau_n$ [24–26]. Presented in Fig. 2 is the snapshot of the sinusoid signal y in (2.1) and its heavily infected samples z_n in (2.2) between 20 and 40 ms via the sampling scheme (2.20). Fig. 3 (a) shows the flow of trajectories in the three-dimensional state space for the system (2.13), where the frequency of a sinusoid signal could be recovered from the system as one of its states, θ. Shown in Fig. 3 is a Poincare section [52] of the system (2.13), where the flow of trajectories of the system (1.3) passes through the section $x_2 = 0$. The attractor plotted in red reveals the periodic flow of trajectories near the true frequency of the input excitation signal in a very noisy environment, cf. the unique periodic orbit in (2.3), provided that the initial

$$\mathbf{X}(T_0) = [y(T_0),\ Dy(T_0),\ \theta(T_0)]^T \tag{2.21}$$

in (2.13) has relative error between its third state $\theta(T_0)$ and the true frequency being less than 10%.

The convergence rate of the discrete system (2.13) depends on the adaptation speed, the true frequency of the sinusoid input, and the relative error between the initial frequency and the true

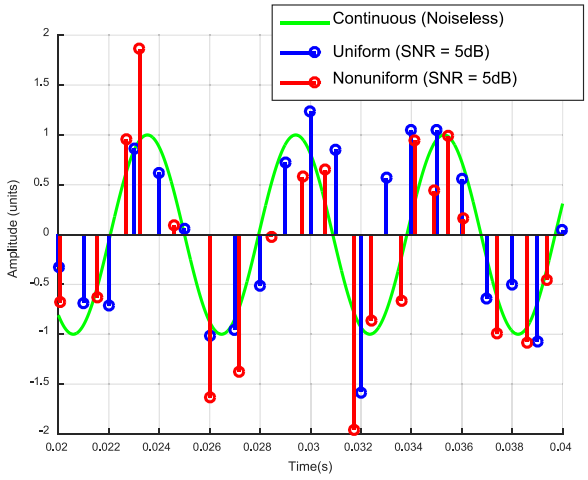

Fig. 2. In the simulation, the signal (plotted in green) has amplitude $A=1$, frequency $f_0 := \theta_0/(2\pi) = 170$ Hz and phase $\phi = \pi/2$, and the samples z_n, corrupted by i.i.d. random noises w_n with SNR = 5 dB, are taken on T_n in (2.20) with $\Delta T = 1$ ms and $\tau_n = 0$ for uniform sampling (plotted in blue) and i.i.d. random $\tau_n \in [.5, 1.5]\Delta T$ for nonuniform sampling (plotted in red). (For interpretation of the references to color in this figure caption, the reader is referred to the web version of this paper.)

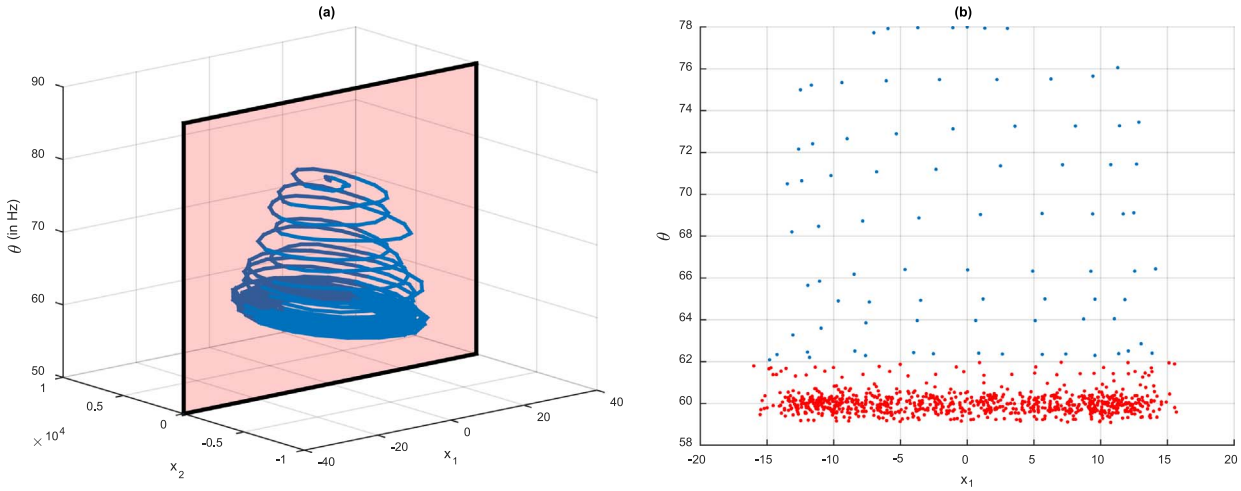

Fig. 3. Flow trajectories and Poincare section of the discrete system (2.13). In the simulation, the sinusoid input y in (2.1) has amplitude $A=1$, frequency $\theta_0 = 120\pi$ and phase $\phi = \pi/2$, the sampling procedure (2.2) is taken uniformly at $T_n = 0.001n$, $0 \le n \le 1000$, seconds with additive i.i.d. random noise w_n at level 5 dB, the notch depth and adaption speed in (1.3) are given by $\xi = 0.15$ and $\gamma = 0.001$, and the approximation order m in (2.13) is 4. (For interpretation of the references to color in this figure, the reader is referred to the web version of this paper.)

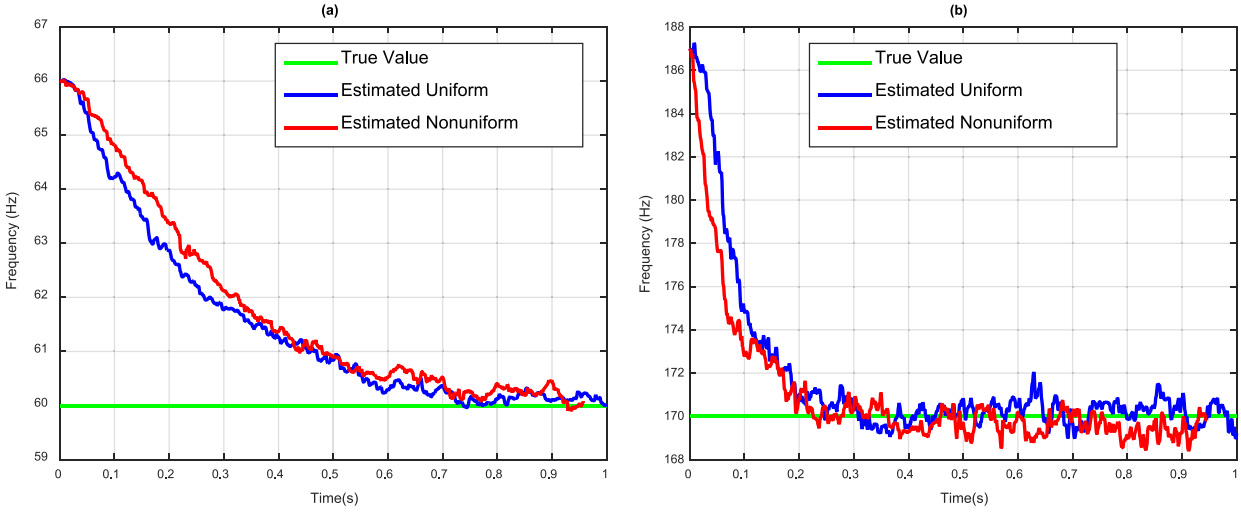

Fig. 4. Convergence of frequency estimation $\theta(T_n)/(2\pi)$ in the discrete ANF method (2.13) to the true frequencies $f_0 := \theta_0/(2\pi)$. In the simulation, the sampling procedure and the input signal y are the same as in Fig. 2 except that $f_0 = 60$ Hz (left) and $f_0 = 170$ Hz (right). The notch depth, adaption speed and approximation order in (1.3) are the same as in Fig. 3.

frequency of the sinusoid input. The frequency estimation in the proposed ANF method (2.13) for two different frequencies, $f_1 = 60$ Hz and $f_2 = 170$ Hz is shown, it is observed to have faster convergence when the true frequency of the input signal is higher, see Fig. 4. Our simulations also indicate that the performance of the algorithm (2.13) degrades gracefully as the SNR of additive noise decreases, see Fig. 5.

The proposed ANF method (2.13) is designed for a single frequency estimation of a sinusoid input. Due to the fast convergence, it could be used to track the frequency change of the input signal,

$$y(n) = \sin[2\pi\tilde{f}\, n\Delta T + \pi/2] \tag{2.22}$$

where the frequency $\tilde{f}$ of the input signal (this frequency is not the true instantaneous frequency but follows a model description for tracking ANF in [40]) changes abruptly due to various reasons, such as power surges, mechanical dysfunction or network disruption. Presented in Fig. 6 is frequency tracking results with uniform sampling gap $\Delta T = 1$ ms, where the frequency of the input signal changes abruptly from 72 Hz to 60 Hz in 1/3 second and from 60 Hz to 80 Hz in the next 1/3 second. It is observed that the corresponding flow trajectory has three periodic orbits, which are near the true frequencies 72 Hz, 60 Hz and 80 Hz of the input signal.

Now, we compare our solution (2.13) of the dynamic system (1.3) with the direct ODE approximation solution. For uniform sampling with time step $h > 0$, the fourth order Runge–Kutta method [54] to solve the system (2.5) is given by

$$\mathbf{X}((n+1)h) = \mathbf{X}(nh) + \frac{h}{6}\Big(\mathbf{Y}_{1,n} + 2\mathbf{Y}_{2,n} + 2\mathbf{Y}_{3,n} + \mathbf{Y}_{4,n}\Big),$$

where

$$\begin{cases} \mathbf{Y}_{1,n} = \mathbf{F}\big(nh, X(nh)\big) \\ \mathbf{Y}_{2,n} = \mathbf{F}\big((n+1/2)h, \mathbf{X}(nh) + \mathbf{Y}_{1,n}h/2\big) \\ \mathbf{Y}_{3,n} = \mathbf{F}\big((n+1/2)h, \mathbf{X}(nh) + \mathbf{Y}_{2,n}h/2\big) \\ \mathbf{Y}_{4,n} = \mathbf{F}((n+1)h, \mathbf{X}(nh) + \mathbf{Y}_{3,n}h), \quad n \ge 0. \end{cases}$$

The above conventional Runge–Kutta method requires the excitation signal y in the continuous form, which could be obtained from its samples (2.2) by certain interpolation. The Runge–Kutta method is not applicable for nonuniform sampling setting, while

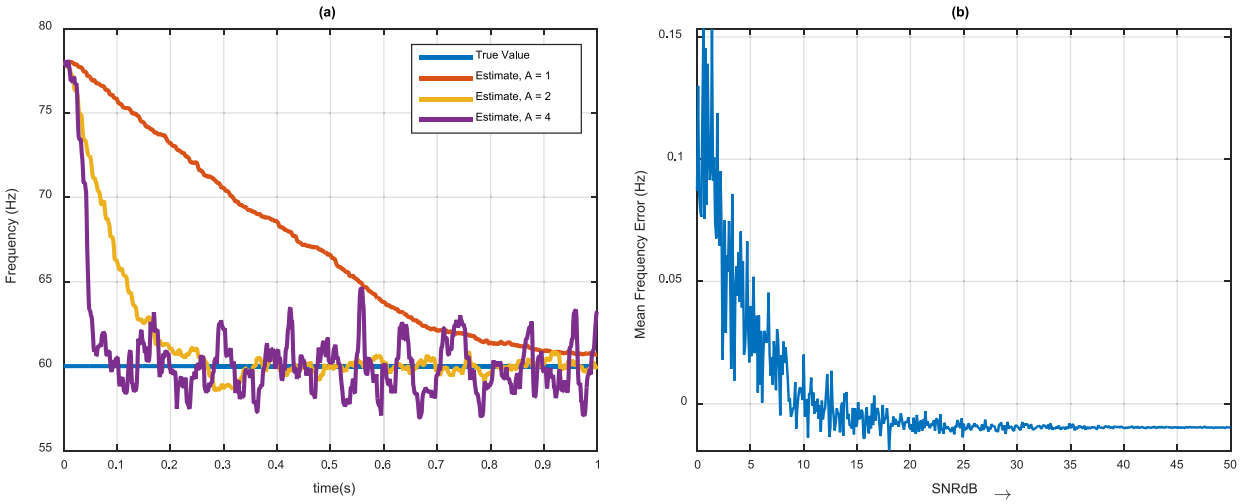

Fig. 5. On the left is frequency estimation $\theta(T_n)/(2\pi)$ of the proposed ANF method for input signals y with different amplitudes, while on the right is mean frequency error of the proposed ANF method for 500 independent trials for each noise level. In the simulation, the signal y, the sampling procedure, and the input signal y, the notch depth, adaption speed and approximation order are the same as in Figs. 2 and 3, except that y has amplitudes $A = 1, 2, 4$ for the left figure, and y has amplitude $A=2$ and SNR of sampling noises w_n varies from 0 to 50 dB for the right figure.

our proposed method (2.13) is designed for a generic nonuniform input data. Even for uniform sampling setting, simulations show that the proposed ANF method (2.13) has slightly faster convergence than the Runge–Kutta method does, and it has better frequency estimation when the input signal has higher frequencies between the two frequencies shown, see Fig. 7. This demonstrates the importance of proper discretization of the continuous dynamic system (1.3), especially when only the noisy nonuniformly sampled data is available.

Finally we compare our technique with the ANF frequency estimation and tracking proposed in [40]. As seen from Fig. 8, using the same signal model as described in (2.22), our method achieves comparable convergence results in purely uniform sampling settings. However, there are several fundamental differences:

- The design of the ANF in [40] is based on a discrete model of filter equations with uniform sampling, while our proposed ANF method works in both uniform and nonuniform sampling setting.
- The design of the ANF in [40] is based on gradient descent (LMS) algorithm of the error function, while our proposed solution is derived from Lyapunov stability analysis and convergence of associated differential equation. The later approach is argued as a superior technique in [1,29].
- The ANF in [40] has only one control parameter, while there are three parameters, the frequency parameter θ, the response tuning parameter λ, and the frequency rejection parameter ξ in our approach. So the ANF in [40] is restricted and it can only estimate the harmonic frequencies, while our approach works for nonharmonic frequency estimation also.
- However there is one advantage due to such simplifying assumption. The ANF in [40] converges to the global minimum, while our proposed solution is proved to have local convergence only.

2.3. Approximation error

Selection of the approximation order m in the proposed ANF method (2.13) depends on the sampling rate, the input signal frequency, the additive noise, and the sampling noise level. In this

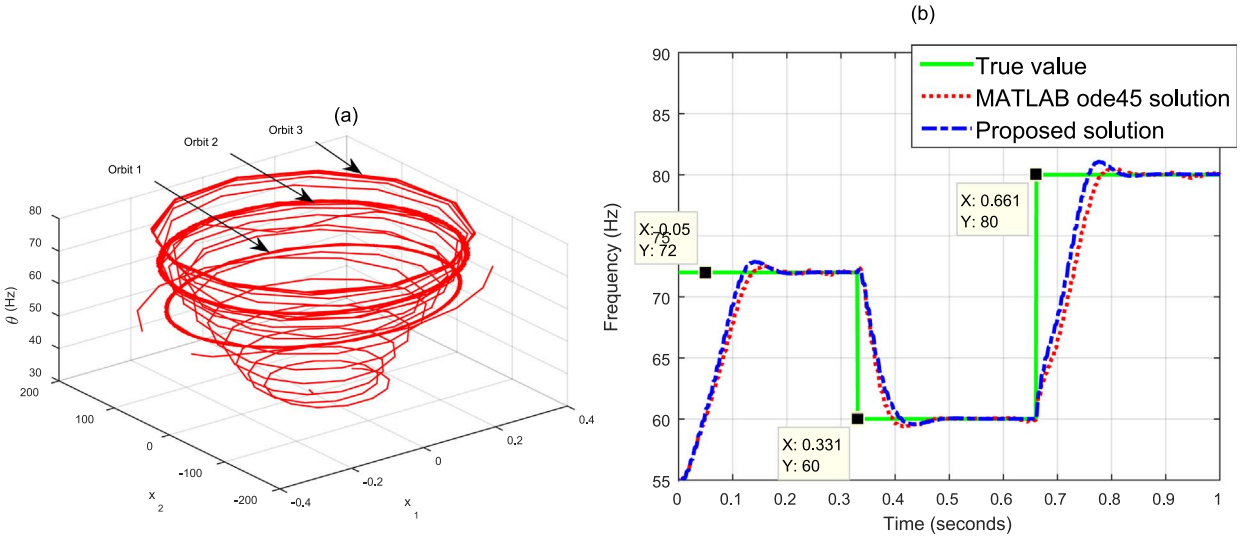

Fig. 6. Frequency tracking of the proposed ANF method (2.13). The sampling procedure (2.2) is taken uniformly at $T_n = 0.001n$, $0 \le n \le 1000$, seconds with additive noise w_n having SNR=20 dB, the adaption speed, $\gamma = 0.01$, and the notch depth, and the approximation order in (1.3) are the same as in Fig. 3.

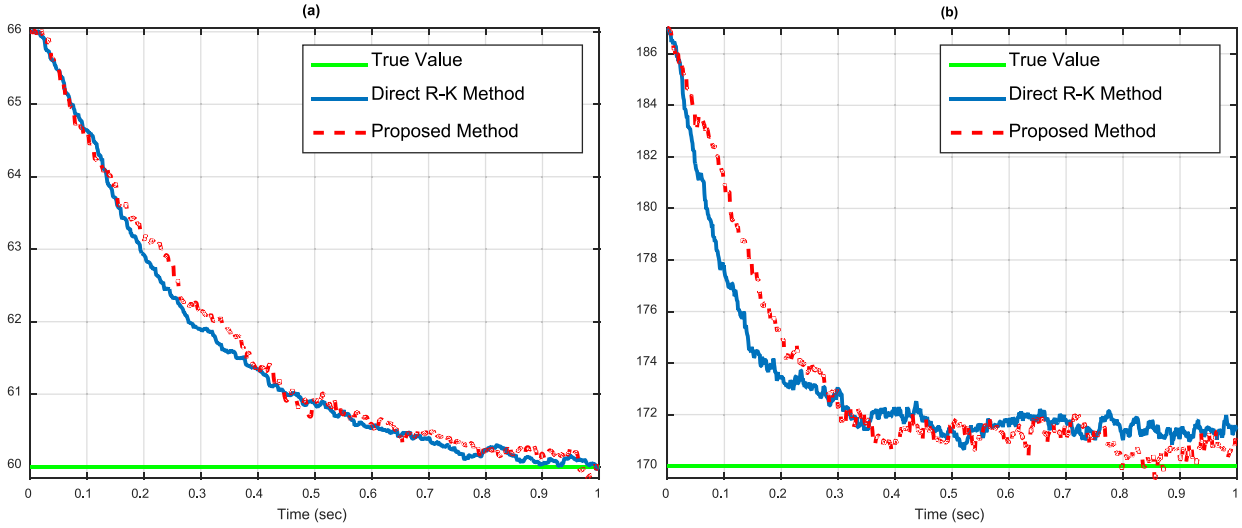

Fig. 7. Comparison between the proposed ANF method (2.13) with $m=4$ and Runge–Kutta method of order 4 on frequency estimation in uniform sampling setting. In this simulation, the input y, the sampling procedure, the notch depth and adaption speed are the same as in Figs. 2 and 3, except that the digital frequency $f_0:=\theta_0/(2\pi)$ of the input signal is 60 Hz for the left figure and 170 Hz for the right figure.

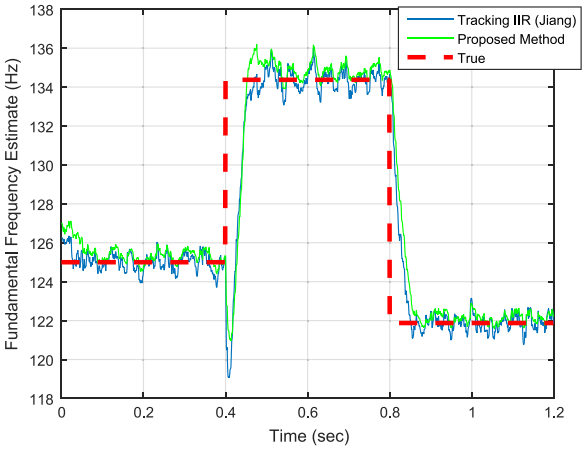

Fig. 8. The sampling procedure (2.2) is taken uniformly at $T_n = 0.001n$, $0 \le n \le 1200$, seconds with additive noise w_n having SNR = 18 dB. The frequency changes abruptly after every 0.4 seconds. The parameters tuned are $\gamma = 0.005$, $\xi = 0.14$ and the ANF is initialize to frequency = 127 Hz. As it is clear that even in purely uniform settings the proposed method which is based on continuous dynamic system has similar speed and accuracy of frequency estimation as the purely discrete model based ANF proposed in [40].

section, we discuss the problem how to choose the approximation order m for mid-range frequency estimation, and consider a combination of the proposed solution with heterodyning technique for high-range frequency estimation. These frequency ranges are specific to the performance of the proposed ANF algorithm, see Section 2.4 for the statistical characterization.

By (2.6), the discrete ANF algorithm (2.13) has approximation error in its discretization being dominated by a multiple of $A(\theta_0 \max_n \Delta T_n)^{m+1}$ for the sinusoidal input $y = A\sin(\theta_0 t + \phi)$ with unknown frequency θ_0. Thus, to achieve better accuracy in the frequency estimation (2.13), one should select the higher approximation order m in the proposed ANF method (2.13).

Observe that

$$\sin(t+\phi) \approx \begin{cases} \left(1 - \frac{t^2}{2!}\right)\sin\phi + t\cos\phi & \text{if } |t| \le \pi/4 \\ \left(1 - \frac{t^2}{2!}\right)\sin\phi + \left(t - \frac{t^3}{3!}\right)\cos\phi & \text{if } |t| \le \pi/3 \\ \left(1 - \frac{t^2}{2!} + \frac{t^4}{4!}\right)\sin\phi + \left(t - \frac{t^3}{3!}\right)\cos\phi & \text{if } |t| \le \pi/2 \end{cases}$$

for all phases ϕ, we may select the approximation order m in the algorithm (2.13) as follows:

$$m = \begin{cases} 2 & \text{if } 0 \le \theta_0 \max_n \Delta T_n \le \pi/4 \\ 3 & \text{if } 0 \le \theta_0 \max_n \Delta T_n \le \pi/3 \\ 4 & \text{if } 0 \le \theta_0 \max_n \Delta T_n \le \pi/2. \end{cases} \tag{2.23}$$

So for estimating frequency of a sinusoid input via the algorithm (2.13) of order m, we need roughly 8 samples per period for $m=2$, 6 samples for $m=3$, and 4 samples for $m=4$, respectively. Our simulations indicate that for an excitation sinusoidal input with its frequency $\theta_0/(2\pi)$Hz larger than 1/8 of sampling rate $1/\max_n \Delta T_n$, it is more reasonable to choose high order approximation in the algorithm (2.13) for its convergence and robustness. For sinusoid input y with low frequency (i.e., $\theta_0 \max_n \Delta T_n$ is not large), a low order approximation in the algorithm (2.13) can be used, while at high frequencies (i.e., $\theta_0 \max_n \Delta T_n$ is large), we observe that $D^3(\theta^2 y)$ of the rescaled input $\theta^2 y$ used in (1.3) could be dominated by the noise, see Fig. 9. From our simulations, we may conclude that the discrete ANF method (2.13) is effective to estimate mid-range frequencies of the input signal which in turn depends on the sampling rate, additive noise and the sampling noise.

When the input signal has high frequency, we can increase the sampling frequency $1/\Delta T$ and that allows us to estimate higher frequency with rapidly sampled data. However when the sampling frequency cannot be increased, we propose to combine the discrete ANF method (2.13) with the heterodyning technique [55]. Take the input excitation signal $y(t) = A\sin(\theta_0 t + \phi)$ with unknown high frequency θ_0, and a modulator frequency θ_c with $\theta_0 - \theta_c$ in the effective range of our technique (2.13). Applying sine and cosine modulators with frequency θ_c to the signal y gives

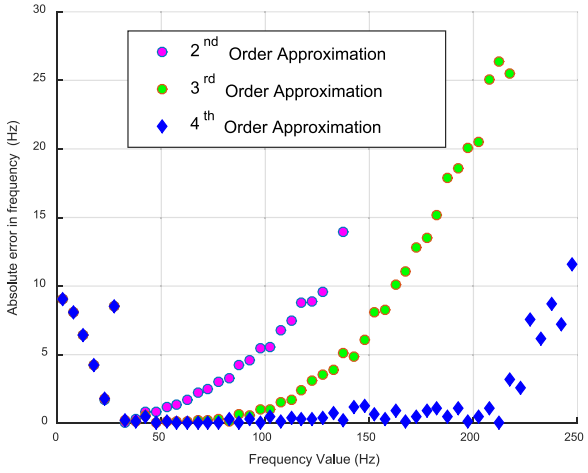

Fig. 9. Frequency estimation of sinusoidal inputs $y=\sin(\theta_0 t+\pi/2)$ with frequencies $\theta_0/(2\pi)$ Hz via the algorithm (2.13) with $m=2$ (squared magenta), $m=3$ (circled green), $m=4$ (diamond shaped blue) respectively. In the simulation, additive jittered sampling is same as shown in Fig. 2. additive noise has SNR=5 dB, and the adaption speed γ and notch depth ξ are 0.001 and 0.15 respectively. (For interpretation of the references to color in this figure caption, the reader is referred to the web version of this paper.)

$$y_1(t)=y(t)\times\sin(\theta_c t)=\frac{A}{2}\cos((\theta_0-\theta_c)t+\phi)-\frac{A}{2}\cos((\theta_0+\theta_c)t+\phi)$$

and

$$y_2(t)=y(t)\times\cos(\theta_c t)=\frac{A}{2}\sin((\theta_0-\theta_c)t+\phi)+\frac{A}{2}\sin((\theta_0+\theta_c)t+\phi).$$

To eliminate high-frequency component, $\theta_0+\theta_c$, of the modulated signals y_1 and y_2, we apply low pass filter such that only the low frequency component $\theta_c-\theta_0$ passes through, which generates

$$\widehat{y_1}\approx\frac{A}{2}\cos((\theta_0-\theta_c)t+\phi)$$

and

$$\widehat{y_2}\approx\frac{A}{2}\sin((\theta_0-\theta_c)t+\phi).$$

As

$$\sqrt{(2\widehat{y_1})^2+(2\widehat{y_2})^2}\approx A,$$

we re-normalize $\widehat{y_1}$ by

$$\tilde{y}_1=\frac{\widehat{y_1}}{\sqrt{(2\widehat{y_1})^2+(2\widehat{y_2})^2}},\tag{2.24}$$

and use $\tilde{y}_1$ to replace y as the input sinusoid signal of our algorithm (2.13), see Fig. 10 for block diagram of the combination of heterodyning and the discrete ANF method.

In the above heterodyning ANF method for high-frequency estimation, we again need some a priori information on frequency θ_0 of the input signal so that we can select a proper modulator frequency θ_c and construct band pass filter blocks to eliminate high-frequency components of modulated signals. This restricts the application of the heterodyning ANF method to the uniform sampling setting only. On the other hand, our signal re-normalization procedure (2.24) makes our heterodyning ANF method almost independent of amplitude of the input signal, which increases the robustness of our procedure. We did simulations with a number of different frequencies in the range 200–450 Hz and obtained similar estimation results, see Fig. 11.

2.4. Statistical characterization

In this subsection, we compare variance of frequency estimation in the discrete ANF method (2.13) with the Cramer–Rao lower bound (CRLB) for the jittered sampling model (2.19). The statistical property will be useful to determine the range of effective frequencies for the proposed ANF, and also the range of frequencies in which the performance of the proposed ANF degrades.

For the additive white Gaussian noise (AWGN) w_n in (1.2) with variance σ^2, the corresponding CRLB $\mathrm{var}(\hat{\theta})$ for any unbiased frequency estimator $\hat{\theta}$ depends on the frequency θ_0 of the excitation sinusoidal input, and it decreases when more sampling data are available [56,57]. In fact,

$$\mathrm{var}(\hat{\theta})\geq\frac{\sigma^2}{\sum_{n=0}^{N-1}\left(\frac{\partial y(T_n)}{\partial\theta}\right)^2}=\frac{(\sigma/A)^2}{\sum_{n=0}^{N-1}T_n^2\cos^2(T_n\theta_0+\phi)}=\frac{2(\sigma/A)^2}{A_N+B_N\cos\phi-C_N\sin\phi}\geq\frac{2(\sigma/A)^2}{A_N+\sqrt{(B_N)^2+(C_N)^2}},\tag{2.25}$$

where

$$A_N=\sum_{n=0}^{N-1}T_n^2,\quad B_N=\sum_{n=0}^{N-1}T_n^2\cos(2T_n\theta_0)$$

and

$$C_N=\sum_{n=0}^{N-1}T_n^2\sin(2T_n\theta_0).$$

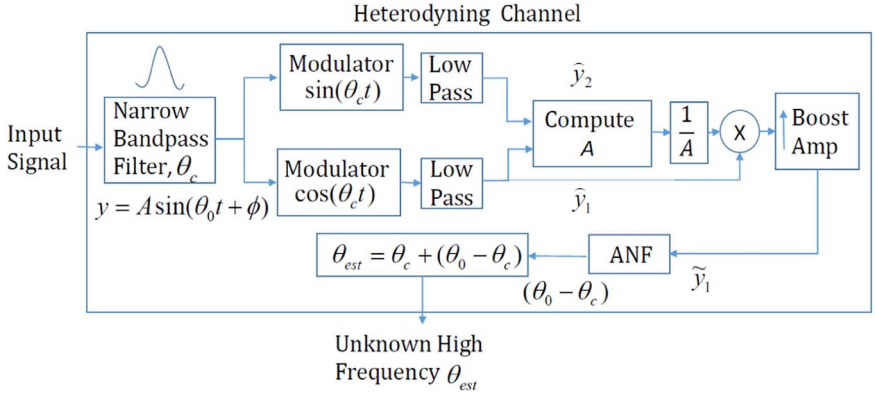

Fig. 10. Block diagram for high frequency estimation.

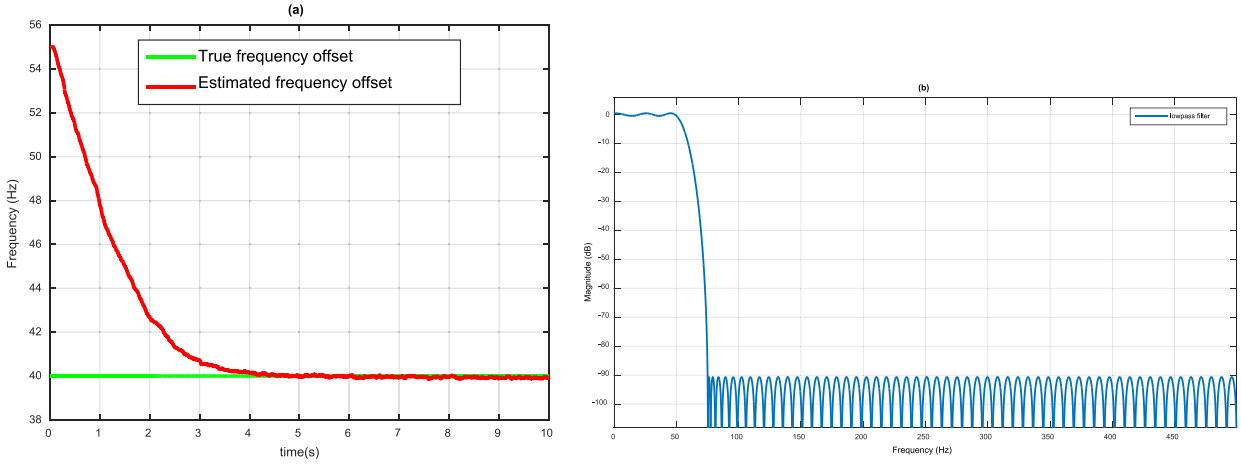

Fig. 11. Heterodyning ANF method for high-frequency estimation. In the simulation, the sinusoid input y, the sampling procedure, the notch depth and adaption speed are the same as in Fig. 3 except that the frequency $f_0 = \theta_0/(2\pi)$ of y is 450 Hz, modulator frequency $f_c = 490$ Hz, and frequency initialization for ANF is 55 Hz. Presented on the right is a lowpass filter using the generic inbuilt MATLAB function fdesign.lowpass with specifications, $F_p = 50$ Hz (passband), $F_{st} = 75$ Hz (stopband), $A_p = 1$, $A_{st} = 90$ (attenuation in dB) with specifications $F_p = 50$ Hz (passband), $F_{st} = 75$ Hz (stopband), $A_p = 1$ dB and $A_{st} = 90$ dB.

From the above estimate (2.25), we see that the CRLB $\mathrm{var}(\hat{\theta})$ may grow without bounds when $T_N\theta_0$ is sufficiently small, cf. Fig. 9, and it is proportional to the signal-noise-ratio σ^2/A^2.

For the uniform sampling between 0 and a seconds (i.e., $T_n = na/N$ seconds for $0 \le n \le N-1$) and the sinusoidal input with positive frequency θ_0, the CRLB $\mathrm{var}(\hat{\theta})$ is asymptotically propositional to reciprocal of the sampling number N,

$$\mathrm{var}(\hat{\theta}) \ge C_0 \frac{(\sigma/A)^2}{N} \tag{2.26}$$

for some positive constant C_0, because

$$\lim_{N\to\infty} \frac{A_N}{N} = \frac{a^2}{3},$$

$$\lim_{N\to\infty} \frac{B_N}{N} = a^2 \int_0^1 x^2 \cos(2a\theta_0 x)dx = a^2\rho_0^{-3}\Big((\rho_0^2 - 2)\sin\rho_0 + 2\rho_0 \cos\rho_0 \Big),$$

and

$$\lim_{N\to\infty} \frac{C_N}{N} = a^2 \int_0^1 x^2 \sin(2a\theta_0 x)dx = a^2\rho_0^{-3}\Big(-2 + (2 - \rho_0^2)\cos\rho_0 + 2\rho_0 \sin\rho_0 \Big),$$

where $\rho_0 = 2a\theta_0$. Thus for the uniform sampling between 0 and a seconds and the sinusoidal input with large frequency θ_0, the CRLB $\mathrm{var}(\hat{\theta})$ is about $6(\sigma/A)^2 a^{-2} N^{-1}$, see Fig. 12.

For a nonuniform sampling between 0 and a seconds with $T_0 = 0$, $T_N = a$ and

$$\max_{1\le n\le N} T_n - T_{n-1} \le \frac{c}{N}$$

for some $c > 0$, we have

$$\frac{A_N}{N} \ge c^{-1} \sum_{n=1}^{N-1} T_n^2 (T_{n+1} - T_n) \to c^{-1} \int_0^a t^2 dt,$$

$$\frac{B_N}{N} \ge c^{-1} \int_0^a x^2 \cos(2\theta_0 x)dx,$$

and

$$\frac{C_N}{N} \ge c^{-1} \int_0^a x^2 \sin(2\theta_0 x)dx$$

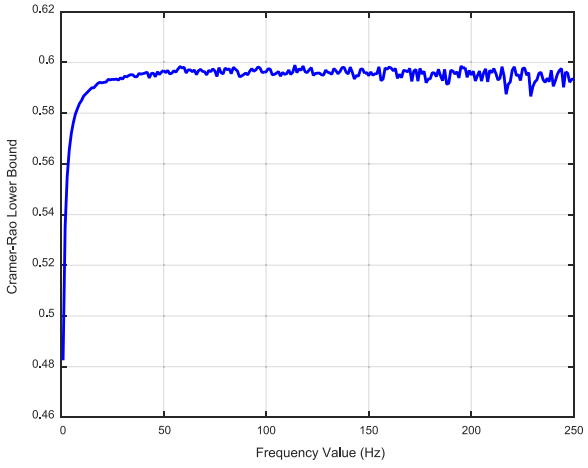

Fig. 12. For jittered sampling $(n + r_n)/1000$, $0 \le n \le 1000$, seconds of sinusoidal inputs $y(t) = \sin(\theta_0 t + \pi/2)$ with frequencies $\theta_0/(2\pi)$Hz, CRLB is about $6(\sigma/A)^2 a^{-2} N^{-1} = 0.6$, where $r_n \in [-1/8, 1/8]$ are randomly selected and the signal-noise ratio $\mathrm{SNR} := 10\log_{10}(\sigma/A)^2$ is 20.

as $N \to \infty$. Hence the asymptotic estimate (2.25) for the CRLB bound $\mathrm{var}(\hat{\theta})$ holds for the above nonuniform setting, including the jittered nonuniform sampling in (2.19) and the additive nonuniform sampling in (2.20).

Due to discretization, the frequency estimate obtained by our proposed method (2.13) is biased, but the systematic error is less than 1% Hz when the input sinusoid has around mid-range frequencies from our simulations, cf. Fig. 5. The variance of frequency estimate is also comparable to the CRLB when the input sinusoid has mid-range frequency, see Fig. 13.

2.5. Extension

In this subsection, we extend the proposed discretization technique in Section 2.1 to continuous dynamic systems for frequency estimation with high accuracy. We apply the extended discretization technique to adaptive notch filtering developed by Mojiri, Xia, Morino, Hou and their collaborators [30–35], and compare their performance on frequency estimation of a sinusoidal input.

Consider a dynamic system

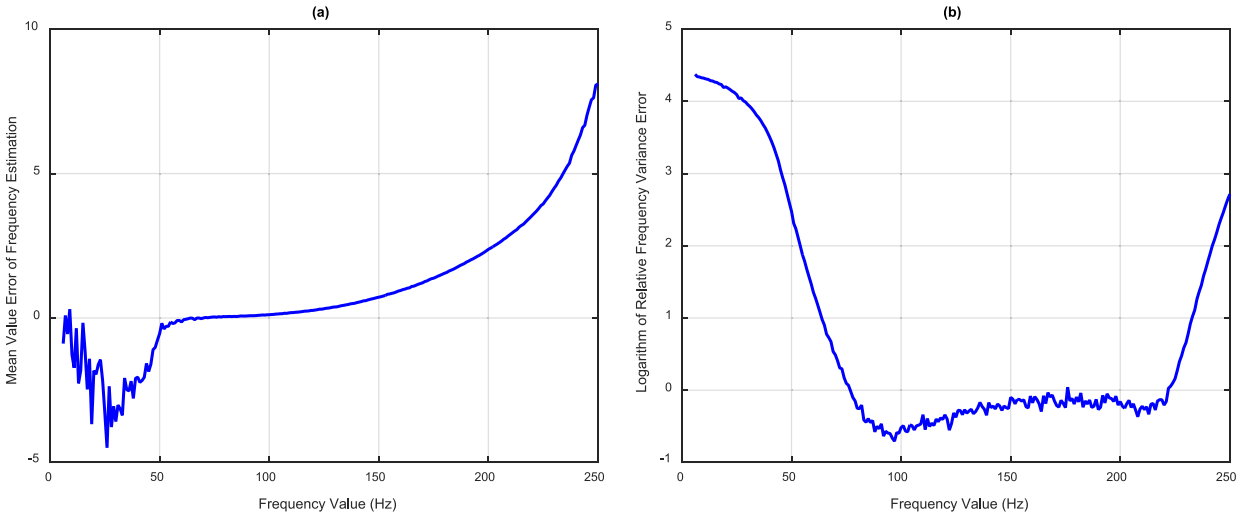

Fig. 13. Listed on the left is the mean value error between the estimated frequency $\theta/(2\pi)$ Hz in the algorithm (2.13) with $m=4$ and the true frequency $\theta_0/(2\pi)$ Hz of the sinusoid input, while on the right is the common logarithm between the variance of the estimated frequency in the algorithm (2.13) and the Cramer–Rao lower bound. In the algorithm (2.13), the jittered sampling set, SNR of the additive noise, the adaption speed and the notch depth are the same as in Fig. 9.

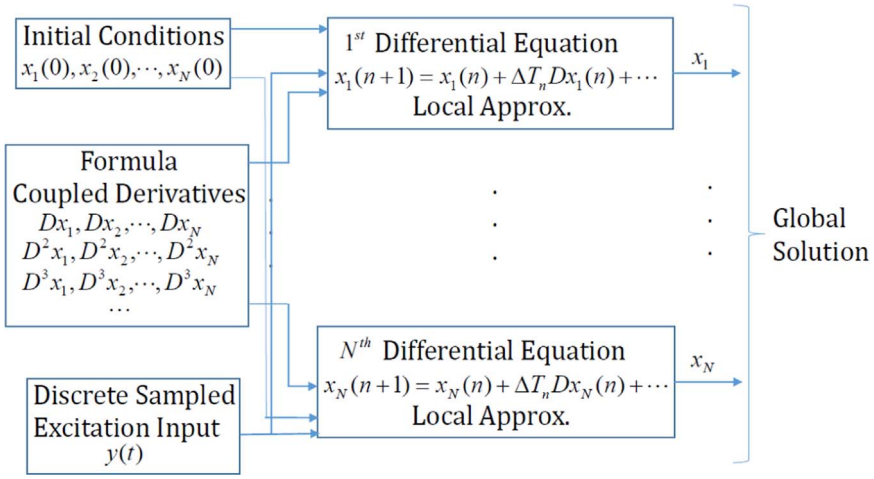

Fig. 14. Block diagram for discretization a dynamic system for frequency estimation.

$$D\mathbf{X} = \mathbf{F}(t, \mathbf{X}, y), \tag{2.27}$$

where $\mathbf{X} = [x_1, x_2, \ldots, x_n]^T \in \mathbb{R}^n$ and $\mathbf{F}$: $\mathbb{R} \times \mathbb{R}^n \times \mathbb{R} \longmapsto \mathbb{R}^n$ is a real analytic function. By the Cauchy–Kovalevskaya theorem [51], the solution $\mathbf{X}(t)$ of the dynamic system (2.27) is analytic and it can been approximated by Taylor polynomials of order $m \geq 0$,

$$\mathbf{X}(t) \approx \sum_{k=0}^{m} \frac{D^k\mathbf{X}(T_n)}{k!}(t - T_n)^k, \quad T_n \leq t \leq T_{n+1}, \tag{2.28}$$

when maximal sampling gap $\max_n(T_{n+1} - T_n)$ is small relative to the changing or stationary signal frequency. In the case that derivatives $D^k y$, $1 \leq k \leq m$, of the input signal y are well approximated at sampling times T_n, $n \geq 0$, we can discretize the dynamic system (2.27) as we did in (2.13) for the system (1.3), see Fig. 14 for the block diagram.

There are several variations for the ANF system (1.3). Mojiri and his collaborators decoupled the notch depth ξ and adaption speed γ in (1.3) [32,34,35], and introduced the following dynamic system:

$$\begin{cases} Dx_1 = x_2 \\ Dx_2 = -2\xi\theta x_2 - \theta^2 x_1 + 2\xi\theta^2 y \\ D\theta = -\gamma(\theta^2 y - \theta x_2)x_1, \end{cases} \tag{2.29}$$

which has a unique periodic orbit,

$$[x_1, x_2, \theta]^T = [-A\cos(\theta_0 t + \phi), A\theta_0 \sin(\theta_0 t + \phi), \theta_0]^T$$

for the sinusoidal input $y = A\sin(\theta_0 t + \phi)$. An additional constraint for stability is $\xi > 1$, hence the notch depth cannot be made very narrow to reject other frequencies unlike the system (1.3).

In [31], Xia observed the similarity between adaptive notch filters and adaptive identifiers, and then he introduced a frequency estimator of fourth order,

$$\begin{cases} Dx_1 = -bx_1 - y \\ Dx_2 = bx_1x_4 + k_1(y - x_3) \\ Dx_3 = x_2 + x_1x_4 + k_2(y - x_3) \\ Dx_4 = \gamma x_1(y - x_3), \end{cases} \tag{2.30}$$

where $b, k_1, k_2, \gamma > 0$. The above dynamic system has globally exponential convergence and its fourth state x_4 converges to squared frequency ${\theta_0}^2$ of the sinusoidal input $y = A\sin(\theta_0 t + \phi)$. Similar frequency estimator of fourth order was introduced by Marino and Tomei [30] independently,

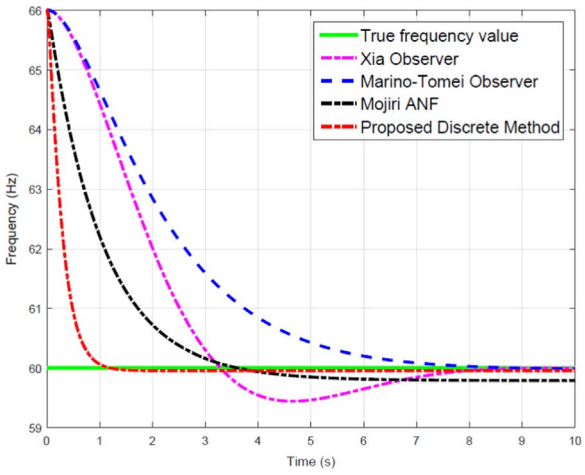

Fig. 15. In this simulation, the input y in (2.1) has amplitude $A=1$, frequency $\theta_0 = 120\pi$ and phase $\phi = \pi/3$, the sampling procedure (2.2) is taken uniformly at $T_n = 0.001n$, $0 \le n \le 1000$, seconds without additive noise w_n, the approximation order m in (2.13) is 4 and initial frequency is about 66 Hz or with 10% error. Also we set $\xi = 0.15$ and $\gamma = 0.001$ in (1.3) and (2.29), $b = 0.3$, $k_1 = k_2 = 0.5$, $\gamma = 0.6$ in (2.30) and $\lambda = 0.4$, $k_1 = 0.5$, $\gamma = 0.6$ in (2.31).

$$\begin{cases} Dx_1 = -\lambda x_1 - y \\ Dx_2 = x_3 + \lambda y + x_1 x_4 + k_1(y - x_2) \\ Dx_3 = -\lambda x_3 - \lambda^2 y \\ Dx_4 = \gamma x_1 (y - x_2), \end{cases} \tag{2.31}$$

where $\lambda, \gamma > 0$ and $k_1 > 1/(4\lambda)$.

For the above dynamic systems (2.29)–(2.31) we may apply similar technique used in (2.12) to approximate $D^k y$, $1 \le k \le m$, of the input signal y at sampling times T_n, $n \ge 0$ or for the uniform sampling we can use Runge–Kutta method directly also. This leads to discretization of those dynamic systems, which is similar to the one (2.13) based on the system (1.3). Our simulations show that the solution of those dynamic systems (2.29)–(2.31) provides the frequency estimate of a sinusoid input y, but comparing with the proposed method based on the dynamic system (1.3), they have slower convergence, see Fig. 15.

3. Multiple frequency estimation

In this section, we introduce two modifications of the discrete ANF technique (2.13) and discuss their performance for multiple frequency estimation of a signal in (1.1) from its noisy nonuniform samples (1.2). We remark that once all frequencies of the signal are retrieved, its amplitudes and phases could be evaluated by finding least squares estimates [59] or directly using the states of some dynamic system by (2.3).

For multiple frequency estimation, adaptive dynamic systems that try to estimate all frequencies at the same time have been proposed but their formulations are very complicated for increasing number of frequencies [44]. As an ideal notch filter has unit gain at all frequencies except at notch frequency where its gain is zero, we may use simple configurations of ANFs tracking only one frequency per channel. Such a configuration could be implemented by applying the discretized ANF technique (2.13) with different initial frequencies, and then approximating the input signal from its noisy samples. If the initial frequencies can be chosen in around the true frequencies, the algorithm (2.13) may lead to accurate approximation of true frequencies of the input signals, but it might only track the dominant frequency (higher amplitude) or the lower frequency of the input signal (since we have higher accuracy estimation for components with lower frequency) effectively, and hence the other frequencies could not be retrieved, see Fig. 16.

The above observation on the frequency retrieval inspires us to introduce the following cascade ANF method:

- First find a notch frequency θ_1 (mostly the dominant one or the lower frequency) of the input signal by applying the discretized ANF method (2.13) or its combination with heterodyning.
- Then extract the sinusoid $y_1 = A_1 \sin(\theta_1 t + \phi_1)$ with that frequency θ_1 from the signal y. The sinusoid $y_1 \approx 2\xi x_1/\theta_1$ by (2.3), where x_1 is the first state of the system (2.13).
- Next, remove that sinusoid from the signal and pass the new signal $y - \hat{y}_1$ to the next stage.
- Finally, repeat the above procedure until the residual error is below certain threshold, or all sinusoids in the input signal are extracted.

The block diagram of the above cascade procedure is presented in Fig. 17, cf. [3] for similar configuration in audio signal processing.

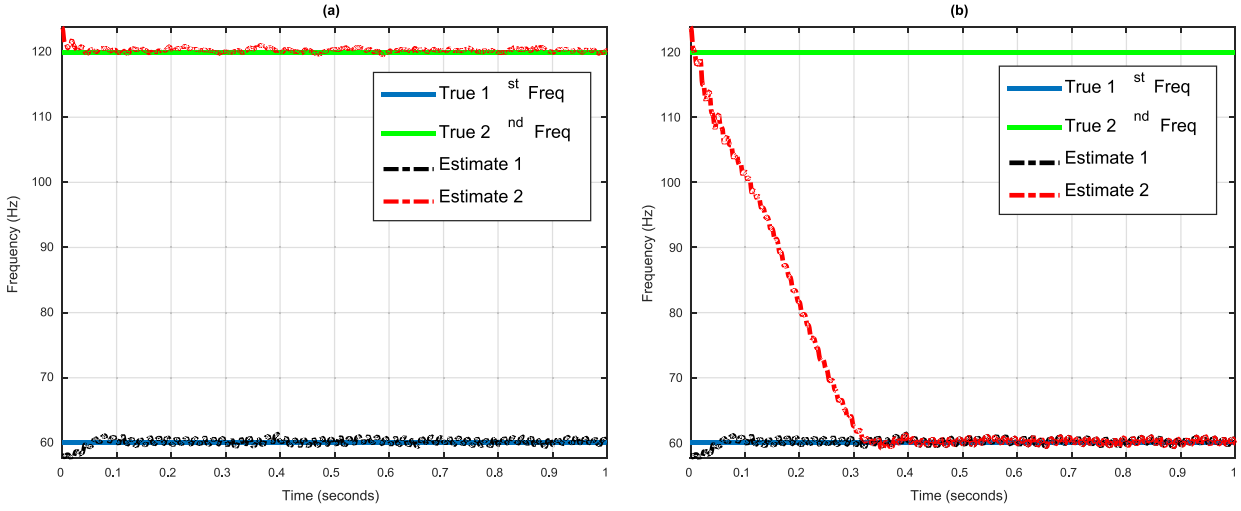

Fig. 16. Frequency retrieval via discrete ANF method (2.13). In the simulation, the sampling procedure, the notch depth and adaption speed are the same as in Figs. 2 and 3, two initial frequencies selected are $f_{c1} = 56$ Hz and $f_{c2} = 125$ Hz, and the input signal $y = A_1 \sin(2\pi f_1 t + \phi_1) + A_2 \sin(2\pi f_2 t + \phi_2)$ has phases $\phi_1 = \pi/2$ and $\phi_2 = \pi/7$, frequencies $f_1 = 60$ Hz and $f_2 = 120$ Hz, and amplitudes $A_1 = 1$, $A_2 = 2$ (left) and $A_2 = 1/2$ (right). In this simulation, the dominant frequencies of the input signals are 120 Hz for the left figure and 60 Hz for the right figure respectively.

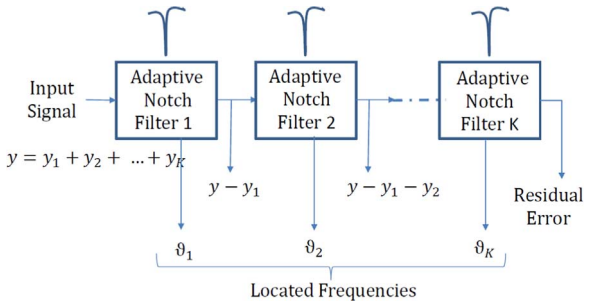

Fig. 17. Block diagram of cascade procedure for multiple frequency estimation.

The cascade procedure is attractive, as applying the discretized ANF technique (2.13) in each stage may retrieve one of the sinusoids, and the remaining stage would have no choice but to seek other sinusoids [36]. However, the disadvantages with the cascade procedure include the distortion introduced by the discretized ANF technique (2.13) at each cascade stage, and the time delay that is introduced due to processing and retrieval of each sinusoidal component. This could render online estimation impractical if the signal y is composed of many frequencies.

To avoid the distortion introduced the discretized ANF technique (2.13) at each cascade stage, we propose an alternative approach to combine our discrete ANF technique (2.13) with band pass prefiltering:

- First, apply band pass filters with some a priori chosen central frequencies, θ_{1c}, θ_{2c}, …, θ_{Kc}, to the samples of the input signal for initial spectral selection.
- Then, use the discretized ANF technique (2.13) for the filtered samples to obtain the true frequencies around the band pass frequencies independently.

The block diagram for parallel implementation of the above discrete ANF technique with prefiltering is presented in Fig. 18, cf. adaptive filtering in [58] for multi-frequency estimation.

By introducing narrow bandpass filters to do the initial spectral selection, we effectively eliminate distortion of the cascade procedure in each stage, while we still embrace the benefits of the parallel implementation for fast sinusoid retrieval.

For uniform sampling procedure, we may design narrow bandpass filters directly (using MATLAB fdesign) or design filter G from the complementary notch filters H, with their transfer functions $G(z)$ and $H(z)$ are related by

$$G(z) = 1 - H(z).$$

For instance, H is a notch filter of second order,

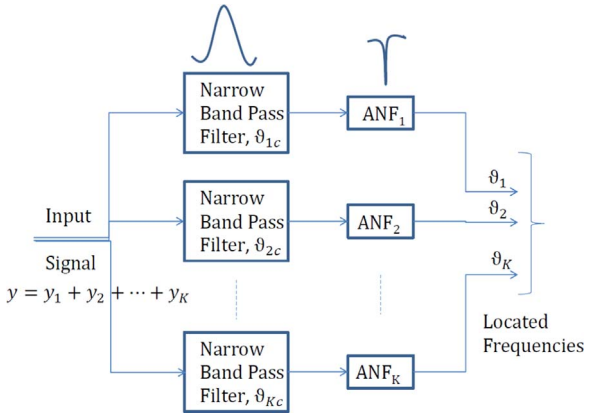

Fig. 18. Block diagram of discrete ANF method with prefiltering.

$$H(z) = \frac{1 - 2\cos(\omega_0)z^{-1} + z^{-2}}{1 - 2r\cos(\omega_0)z^{-1} + r^2 z^{-2}} \tag{3.1}$$

with notch bandwidth parameter $r \in (0, 1)$ and notch frequency ω_0.

The drawback of prefiltering ANF method is that narrow band prefiltering is not applicable when only nonuniform sampling of the input signal is available.

The rest of this section is devoted to demonstration of the cascade ANF procedure and the prefiltering ANF procedure to estimate multiple frequencies of the multi-sinusoid signals effectively in various settings.

3.1. Inputs with two well-separated frequencies

Consider an input signal

$$y = A_1 \sin(2\pi f_1 t + \phi_1) + A_2 \sin(2\pi f_2 t + \phi_2) \tag{3.2}$$

with its two frequencies $f_1 f_2$ being far away. Our simulations show that both prefiltering ANF and cascade ANF provide estimations close to true frequencies of the input signal y, see Fig. 19 and cf. Fig. 16.

For uniform sampling setting, prefiltered configuration is a bit more suitable in terms of both speed and accuracy, but in nonuniform sampling we can effectively use cascade configuration especially when there are small number of frequencies for the input signal.

3.2. Input with two very close frequencies, a pathological case

Consider an input signal y of the form (3.2) with its two frequencies f_1 and f_2 being close. As those two frequencies cannot be separated using narrow band pre-filters especially in highly noisy sampling environment, prefiltering ANF method does not provide reasonable frequency estimations. So in this subsection, we restrict ourselves to discuss frequency estimation via the cascade ANF method in that pathological case.

In order to reject one frequency from the other, we should select small notch depth ξ in (1.3). Therefore by (2.4), the adaption speed γ in the dynamic system (1.3) should be small too, which implies that the discrete dynamic system (2.13) has slow convergence and there are long delay to retrieval of true frequencies. Our simulations indicate that it is better to select the first initial frequency in the middle of those two close frequencies if we do not have much information on the dominant frequency, see Fig. 20 and cf. Fig. 16.

Most of known frequency estimations has poor performance for the pathological case, see [50] and references therein. What is unexpected to select slow adaption speed and narrow notch depth is the robustness of our frequency estimation. We did the simulation for noise with SNR=40, 30, 20, 10, 0 dB, and in all cases we get the same consistent and smooth estimates. Possible reasons for such phenomenon could be that the ANF has excellent noise rejection capability especially when we make the adaptation speed slow and the filter bandwidth narrow. This could make our cascade ANF method more powerful than the one in [7], where it is required that the signal power must be greater than the noise power in their methods.

3.3. Input with multiple harmonic frequencies

Consider an input signal

$$y = \sum_{k=1}^{K} A_k \sin(\theta_k t + \phi_k) \tag{3.3}$$

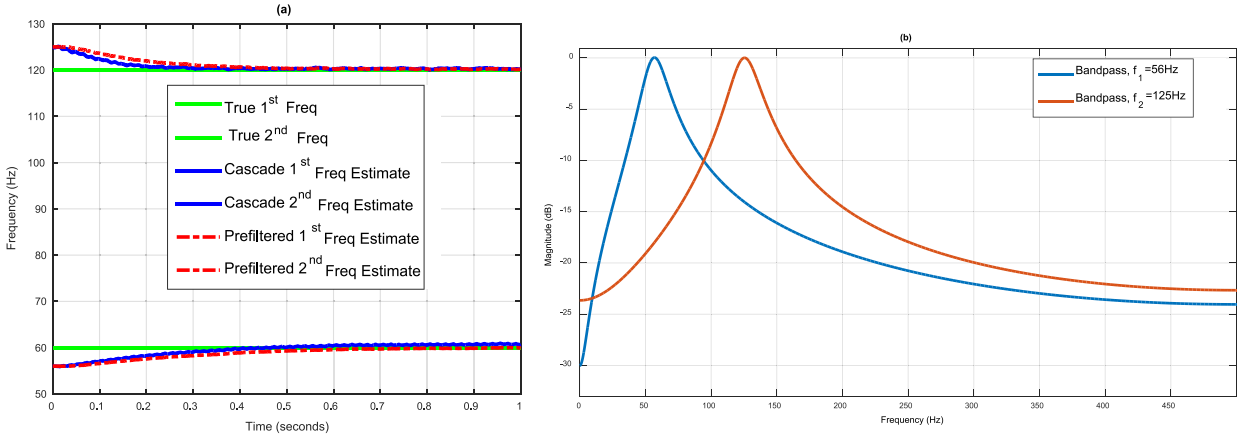

Fig. 19. Frequency estimation via prefiltering ANF and cascade ANF methods. In this simulation, the sampling procedure, the notch depth and adaption speed, and two initial frequencies selected are the same as in Fig. 16, and the signal y in (3.2) has amplitudes $A_1 = 1$ and $A_2 = 2$, phases $\phi_1 = \pi/2$ and $\phi_2 = \pi/7$, and frequencies $f_1 = 60$ Hz and $f_2 = 120$ Hz. Plotted on the left is frequency estimation via cascade ANF method (in solid blue line) and prefiltering ANF method (in dashed red line), while plotted on the right is narrow band pass prefilter around two initial frequencies being used in the prefiltering ANF method. (For interpretation of the references to color in this figure caption, the reader is referred to the web version of this paper.)

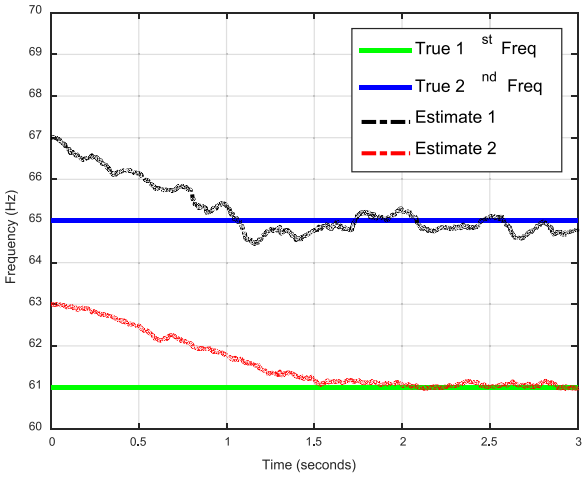

Fig. 20. Frequency retrieval of inputs with two close frequencies via the cascade ANF method. In this simulation, the input signal y in (3.2) has frequencies $f_1 = 61$ Hz (dominant frequency for the right figure), $f_2 = 65$ Hz (dominant frequency for the left figure), phases $\phi_1 = \pi/2$, $\phi_2 = \pi/7$, and amplitude $A_1 = A_2 = 1$, the sampling procedure is the same as in Fig. 19 except sampling time interval is $[0, 3]$ second, the adaption speed $\gamma = 0.00001$ (one hundredth of the one in Fig. 19), and notch depth $\xi = 0.015$ (one tenth of the one in Fig. 19), the first initial frequency is 63 Hz (mean values of f_1 and f_2), and 67 Hz (about 5% above the non-dominant frequency f_2).

with harmonic frequencies $\theta_k = k\theta_1$, $2 \le k \le K$ [59]. For a signal with harmonic frequencies, it suffices to find its fundamental frequency $\theta_1/(2\pi)$ Hz, which could be obtained by bandpass filtering of the input signal. We observe that the fundamental frequency can be estimated consistently via a single ANF block in a highly noisy environment. Presented in Fig. 21, cf. Fig. 6, is the fundamental frequency estimation of the signal y in (3.3) with amplitudes $A_1 = 1, A_2 = A_1/2, A_3 = A_1/3, A_4 = A_1/4, A_5 = A_1/5$, phases $\phi_k \in [0, \pi]$ randomly selected, and fundamental frequency f_0 changing abruptly from 72 Hz to 60 Hz at 1/3 second and from 60 Hz to 80 Hz at 2/3 second, cf. signals with time-varying fundamental frequency in power systems [59]. The above observation makes our solution very suitable for time domain signal analysis similar to [60] (which is a CT system), but now we can do it with nonuniformly sampled data in the presence of random sampling noise and additive noise.

3.4. Input with multiple frequencies

In this subsection, we consider frequency estimation when input signals (1.1) have multiple frequencies. Due to the distortion by cascade ANF in each iteration, we propose to apply prefiltering ANF method for frequency estimation. Presented in Fig. 22 is a demonstration for our prefiltering ANF frequency estimator, where the input signal

$$y = \sum_{k=1}^{7} A_k \sin(2\pi f_k t + \phi_k)$$

has amplitudes $A_k \in [0.5, 1.5]$ and phases $\phi_k \in [-\pi, \pi]$, $1 \le k \le 7$, being randomly selected, and the actual frequencies are $(f_1, \ldots, f_7) = (78, 137, 177, 234, 288, 325, 437)$ Hz.

4. Conclusions

Multiple frequency estimators from nonuniform sampling data are proposed in this paper, which reconcile the merits of adaptive notch filtering in continuous time while restricting to operate directly on discrete time data. Despite the mathematical difficulties, some conclusive results on the local stability analysis and convergence of the proposed solution are established. To our best knowledge, solving the frequency estimation problem directly from some dynamic systems is not presented in the literature when only nonuniform sampling data are available. We expect that this paper will stimulate further interest in this direction.

Local stability analysis, convergence and the stochastic characterization of the proposed frequency estimators are established when the input signal has single frequency. Extensive simulations for various scenarios demonstrate robustness, accuracy and fast tracking of the proposed frequency estimators. For multiple frequencies, we have two proposed methods, the cascade procedure and the prefiltering process. While the cascade method is good for small number of frequencies in nonuniform setting, the prefiltering method is useful for faster response in uniform settings. The proposed method is robust even in the estimation of two close frequencies in high noise.

Further research on parameter tuning, which is an open problem in control research, especially for particular applications of the proposed frequency estimators to signal processing and control, is needed. The reader may refer to [29–35] on robust parameter tuning for adaptive notch filtering in the continuous domain.

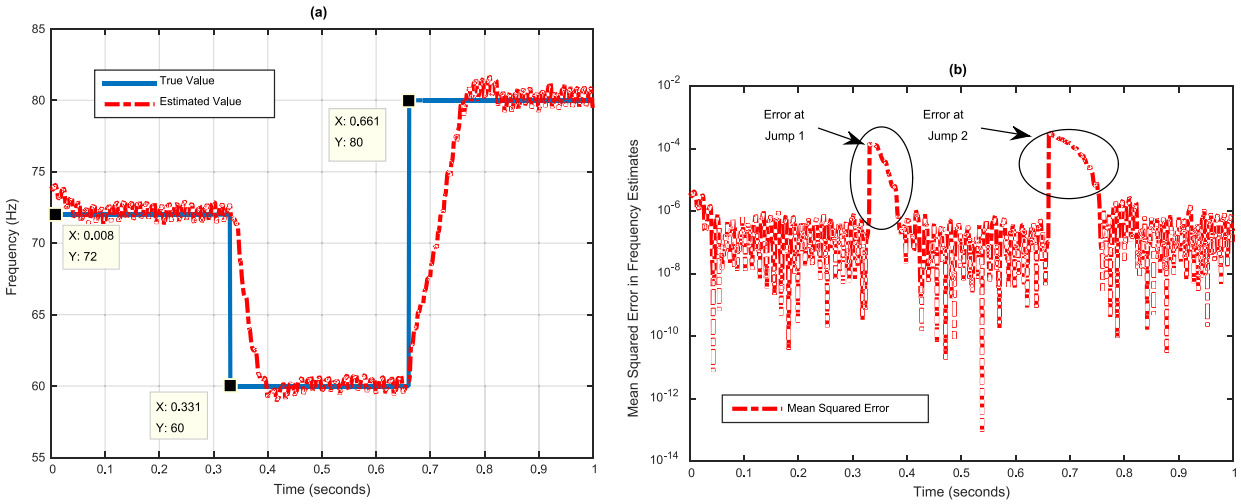

Fig. 21. Fundamental frequency tracking of an input signal with harmonic frequencies using a single ANF block. In the simulation, the sampling procedure, notch depth, adaption speed and initial frequency are the same as the ones in Fig. 6(b).

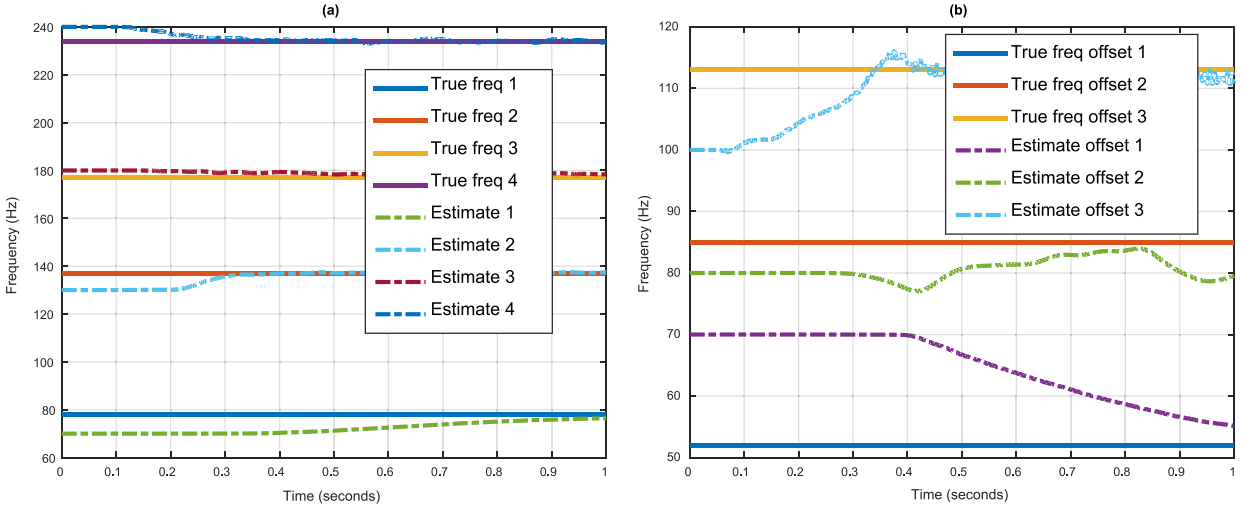

Fig. 22. In the simulation, the sampling procedure, the notch depth and adaption speed are the same as in Fig. 16. Presented on the left is the first four frequency estimation via the prefiltering ANF method (2.13) with the initial frequencies 70, 130, 180, 240 Hz. On the right is the last three frequency estimation via discrete ANF method with heterodyning, where we use 270, 330, 450 Hz as center frequencies of bandpass filters.

Acknowledgment

The authors would like to thank the anonymous reviewers for their valuable comments and suggestions to improve the quality of the paper, and in the spirit of reproducible research we make our code freely available to the public @https://github.com/syedalamabbas/NonUniformSamplesAdaptiveNotchFilter.

References

[1] P.A. Regalia, An improved lattice-based adaptive IIR notch filter, IEEE Trans. Signal Process. 39 (1991) 2124–2128.
[2] C. Fuller, A.V. Flotow, Active control of sound and vibration, IEEE Control Syst. Mag. 15 (1996) 9–19.
[3] A.P. Klapuri, Multiple fundamental frequency estimation based on harmonicity and spectral smoothness, IEEE Trans. Speech Audio Process. 11 (2003) 804–816.
[4] O. Simeone, Y. Bar-Ness, U. Spagnolini, Pilot-based channel estimation for OFDM systems by tracking the delay-subspace, IEEE Trans. Wirel. Commun. 3 (2004) 315–325.
[5] S.F. Hsieh, K.J.R. Liu, K. Yao, Estimation of multiple sinusoidal frequencies using truncated least squares methods, IEEE Trans. Signal Process. 41 (1993) 990–994.
[6] R. Badeau, B. David, G. Richard, High-resolution spectral analysis of mixtures of complex exponentials modulated by polynomials, IEEE Trans. Signal Process. 54 (2006) 1341–1350.
[7] Q. Zhang, L.J. Brown, Noise analysis of an algorithm for uncertain frequency identification, IEEE Trans. Autom. Control 51 (2006) 103–110.
[8] K.M. Ghartemani, B.T. Ooi, A. Bakhshai, Application of enhanced phase-locked loop system to the computation of synchrophasors, IEEE Trans. Power Deliv. 26 (2011) 22–32.
[9] A. Dutt, V. Rokhlin, Fast Fourier transforms for nonequispaced data, SIAM J. Sci. Comput. 14 (1993) 1368–1393.
[10] P. Stoica, R.L. Moses, Introduction to Spectral Analysis, Prentice-Hall, Englewood Cliffs, NJ, 1997.
[11] P. Stoica, E.G. Larsson, J. Li, Adaptive filterbank approach to restoration and spectral analysis of gapped data, Astron. J. 120 (2000) 2163–2173.
[12] F. Marvasti, Nonuniform Sampling: Theory and Practice, vol. 1, Kluwer Academic/Plenum Publishers, New York, 2001, https://www.springer.com/us/book/9780306464454.
[13] F. Eng, Non-uniform sampling in statistical signal processing (Ph.D. thesis), 2007.
[14] M.W. Maciejewski, H.Z. Qui, I. Rujan, M. Mobli, J.C. Hoch, Nonuniform sampling and spectral aliasing, J. Magn. Reson. 1 (2009) 88–93.
[15] R.L. Cook, Stochastic sampling in computer graphics, ACM Trans. Graph. (TOG) 5.1 (1986) 51–72.
[16] S. Trittler, F.A. Hamprecht, Near optimum sampling design and an efficient algorithm for single tone frequency estimation, Digit. Signal Process. 19 (2009) 628–639.
[17] A. Holland, M. Aboy, A novel recursive Fourier transform for nonuniform sampled signals: application to heart rate variability spectrum estimation, Med. Biol. Eng. Comput. 47 (2009) 697–707.
[18] J.A. Gansman, J.V. Krogmeier, M.P. Fitz, Single frequency estimation with non-

uniform sampling, in: IEEE Asilomar Conference Signals, Systems and Computers, vol. 1, 1996, pp. 399–403.
[19] Y.C. Eldar, A.V. Oppenheim, Filterbank reconstruction of bandlimited signals from nonuniform and generalized samples, IEEE Trans. Signal Process. 48 (2000) 2864–2875.
[20] H. Johansson, P. Lowenborg, Reconstruction of nonuniformly sampled bandlimited signals by means of digital fractional delay filters, IEEE Trans. Signal Process. 50 (2002) 2757–2767.
[21] R.S. Prendergast, C.L. Bernard, P.J. Hurst, Reconstruction of band-limited periodic nonuniformly sampled signals through multirate filter banks, IEEE Trans. Circuits Syst. 51 (2004) 1612–1622.
[22] A. Tarczynski, N. Allay, Spectral analysis of randomly sampled signals: suppression of aliasing and sampler jitter, IEEE Trans. Signal Process. 52 (12) (2004).
[23] D. Qu, A. Tarczynski, A novel spectral estimation method by using periodic nonuniform sampling, in: IEEE Asilomar Conference Signals, Systems and Computers, 2007, pp. 1134–1138.
[24] M. Unser, Sampling-50 years after Shannon, in: Proceedings of IEEE, vol. 88, 2000, pp. 569–587.
[25] A. Aldroubi, K. Gröchenig, Nonuniform sampling and reconstruction in shift-invariant spaces, SIAM Rev. 43 (2001) 585–620.
[26] Q. Sun, Non-uniform average sampling and reconstruction of signals with finite rate of innovation, SIAM J. Math. Anal. 38 (2006) 1389–1422.
[27] P. Handel, A. Nehorai, Tracking analysis of an adaptive notch filter with constrained poles and zeros, IEEE Trans. Signal Process. 42.2 (1994) 281–291.
[28] M.V. Dragosevic, S.S. Stankovic, An adaptive notch filter with improved tracking properties, IEEE Trans. Signal Process. 43 (1995) 2068–2078.
[29] L. Hsu, R. Ortega, G. Damm, A globally convergent frequency estimator, IEEE Trans. Autom. Control 44 (1999) 698–713.
[30] R. Marino, P. Tomei, Global estimation of n unknown frequencies, IEEE Trans. Autom. Control 47 (2002) 1324–1328.
[31] X. Xia, Global frequency estimation using adaptive identifiers, IEEE Trans. Autom. Control 47 (2002) 1188–1193.
[32] M. Mojiri, A.R. Bakhshai, An adaptive notch filter for frequency estimation of a periodic signal, IEEE Trans. Autom. Control 49 (2004) 314–318.
[33] M. Hou, Amplitude and frequency estimator of a sinusoid, IEEE Trans. Autom. Control 50 (2005) 855–858.
[34] M. Mojiri, A.R. Bakhshai, Stability analysis of periodic orbit of an adaptive notch filter for frequency estimation of a periodic signal, Automatica 43 (3) (2007) 450–455.
[35] M. Mojiri, M.K. Ghartemani, A. Bakhshai, Estimation of power system frequency using an adaptive notch filter, IEEE Trans. Instrum. Meas. 56 (2007) 2470–2477.
[36] P. Regalia, Adaptive IIR Filtering in Signal Processing and Control, CRC Press, 1994, .
[37] D. Victor, S. Torres, Multiple fully adaptive notch filter design based on allpass sections, IEEE Trans. Signal Process. 48 (2000) 550–552.
[38] Y.C. Lim, Y.X. Zou, N. Zheng, A piloted adaptive notch filter, IEEE Trans. Signal Process. 53 (2005) 1310–1323.
[39] J.E. Cousseau, S. Werner, P.D. Donate, Factorized all-pass based IIR adaptive notch filters, IEEE Trans. Signal Process. 55 (2007) 5225–5236.
[40] L. Tan, J. Jiang, Novel adaptive IIR notch filter for frequency estimation and tracking, IEEE Signal Process. Mag. 26 (2009) 186–189.
[41] P.A. Regalia, A complex adaptive notch filter, IEEE Signal Process. Lett. 17 (2010) 937–940.
[42] M. Bodson, S.C. Douglas, Adaptive algorithms for the rejection of sinusoidal disturbances with unknown frequency, Automatica 33 (1997) 2213–2221.
[43] G. Damm, L. Hsu, R. Ortega, The effect of noise on a global frequency estimator, in: Proceedings of MTNS, Padova, Italy, 1998.
[44] M. Hou, Parameter identification of sinusoids, IEEE Trans. Autom. Control 50 (2013) 855–858.
[45] G.P. Rao, H. Unbehauen, Identification of continuous-time systems, in: IEE Proceedings in Control Theory and Applications, vol. 153, no. 2, IET, 2006, pp. 185–220, http://ieeexplore.ieee.org/xpl/login.jsp?tp=&arnumber=1595896&url=http%3A%2F%2Fieeexplore.ieee.org%2Fiel5%2F2193%2F33574%2F01595896.pdf%3Farnumber%3D1595896.
[46] H. Garnier, L. Wang, Identification of Continuous-time Models from Sampled Data, Springer, London, 2008.
[47] C.C. Tseng, Design of fractional order digital FIR differentiators, IEEE Signal Process. Lett. 3 (2001) 77–79.
[48] A. Papoulis, Signal Analysis, McGraw-Hill Companies, May 1977, http://www.amazon.com/Signal-Analysis-Athanasios-Papoulis/dp/0070484600.
[49] K. Cheung, R.J. Marks, Ill-posed sampling theorems, IEEE Trans. Circuits Syst. 32 (5) (1985) 481–484.
[50] M. Shahram, P. Milanfar, On the resolvability of sinusoids with nearby frequencies in the presence of noise, IEEE Trans. Signal Process. 53 (2005) 2579–2588.
[51] L.C. Evans, Partial Differential Equations, American Mathematical Society, 1998, http://www.amazon.com/Partial-Differential-Equations-Graduate-Mathematics/dp/0821849743.
[52] S. Lynch, Dynamical Systems with Applications using MATLAB, Springer, 2004, .
[53] Hassan K Khalil, Nonlinear Systems, vol. 3, Prentice Hall, Upper Saddle River, 2002.
[54] R.L. Burden, J.D. Faires, Numerical Analysis, 9th edition, Brooks-Cole, 2010, http://www.cengage.com/search/productOverview.do;jsessionid=27A7AB56619AFF3E7CA0FD5570CBB2CE?N=16+4294948945&Ntk=P_EPI&Ntt=191876703063358196314313487892378522 75&Ntx=mode%2Bmatchallpartial.
[55] H. Robert, M.E. Jernigan, Self-adjusting beat detection and prediction in music, in: IEEE International Conference Proceedings on Acoustics, Speech, and Signal Processing (ICASSP'04), vol. 4, 2004.
[56] S.M. Kay, S.L. Marple Jr., Spectrum analysis – a modern perspective, in: IEEE Proceedings, vol. 69, 1981, pp. 1380–1419.
[57] S.M. Kay, Fundamentals of Statistical Signal Processing, vol. III: Practical Algorithm Development, vol. 3, Pearson Education, 2013, http://www.amazon.com/Fundamentals-Statistical-Signal-Processing-Estimation/dp/0133457117.
[58] E.G. Larsson, P. Stoica, J. Li, Spectral estimation via adaptive filterbank methods: a unified analysis and a new algorithm, Signal Process. 82 (2002) 1991–2001.
[59] S.A. Abbas, A new fast algorithm to estimate real time phasors using adaptive signal processing, IEEE Trans. Power Deliv. 28 (2013) 807–815.
[60] M. Mojiri, M.K. Ghartemani, A. Bakhshai, Time-domain signal analysis using adaptive notch filter, IEEE Trans. Signal Process. 55 (2007) 85–93.